EXPERIMENTS AND SIMULATION OF FLEXURAL-SHEAR DOMINATED RC BRIDGE PIERS UNDER REVERSED CYCLIC LOADING

B.J. Si[1], Z.G. Sun[2], Q.H. Ai[3], D.S. Wang[4] and Q.X. Wang[5]

[1] *Associate Professor, School of Civil & Hydraulic Engineering, Dalian University of Technology, Dalian, China*

[2] *Master,Institute of Road and Bridge Engineering, Dalian Maritime University, Dalian, China*

[3] *Ph.D student, School of Civil & Hydraulic Engineering, Dalian University of Technology, Dalian, China*

[4] *Professor, Institute of Road and Bridge Engineering, Dalian Maritime University, Dalian, China*

[5] *Professor, School of Civil & Hydraulic Engineering, Dalian University of Technology, Dalian, China*

Email: sibingjun@sina.com

ABSTRACT :

In recent earthquakes, a large number of reinforced concrete (RC) bridges were severely damaged as a result of a mixed flexural-shear failure of the bridge piers. An integrated experiment and analysis research program is undertaken in this paper to study the seismic performance of flexural-shear dominated RC bridge piers. In the first part, cyclic loading tests on 6 RC bridge piers were carried out experimentally. The damage states, ductility, and energy dissipation of the piers were compared with each other. In the second part, modeling approaches describing the hysteretic response of the piers were investigated by using ANSYS software. A set of model with different parameters was selected and evaluated through comparison with experimental results. Then, a modified analysis model is presented and the accuracy of the model has been verified by comparing the calculated results with experimental ones.

KEYWORDS: RC bridge piers, flexural-shear failure, finite element, ANSYS software

1. INTRODUCTION

In recent earthquakes, such as 1994 Northridge earthquake, 1995 Kobe earthquake and 1999 Chi-Chi earthquake, a large number of reinforced concrete (RC) bridges were severely damaged as a result of a mixed flexural-shear failure of the bridge piers. To study the seismic performance of the piers with flexural-shear failure mode, a nonlinear cyclic loading test on 6 RC bridge piers with circular cross sections was carried out experimentally, then, modeling approaches describing the hysteretic performance of the piers were investigated by using ANSYS software.

2. EXPERIMENTAL STUDY

2.1. Test Unit Details

Six model RC bridge piers representing about 1/3 scale of the prototype bridge piers were designed, which were designated as A1, A2, A3, A4, A5 and A6, respectively. Figure 1 shows the details of the specimens. Table 1 lists the properties of the specimens.

Measured yield and ultimate strengths of the Φ14 longitudinal bars were 327.6 and 534.9 MPa, respectively. Measured yield and ultimate strengths of ¢6 transverse bars were 511 and 558.9 MP, respectively.

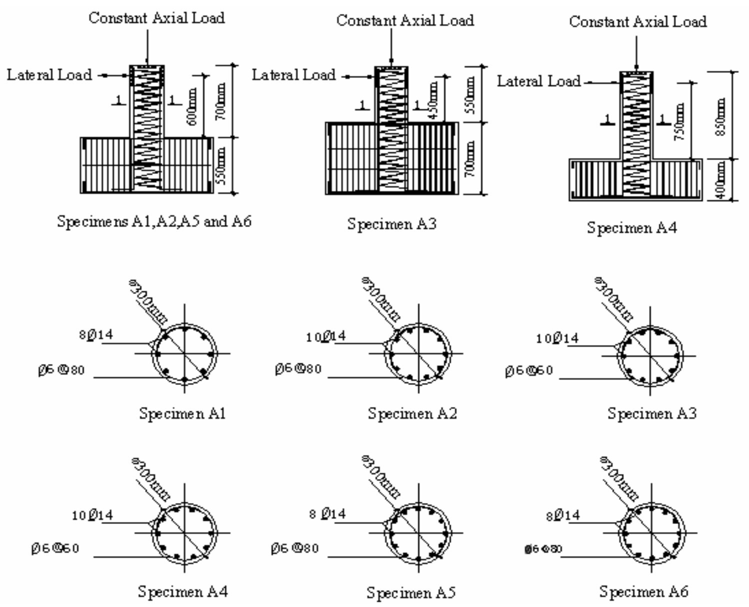

Figure 1 Details of the pier specimens

Table 1 Pier design details

Specimen	Diameter, D (mm)	Aspect ratio	f_c' (MPa)	Longitudinal reinforcement		Transverse reinforcement		Axial load ratio, $P/A_g f_c'$
				Quantity	ρ_t	s (mm)	ρ_s	
A1	300	2	29.4	8Φ14	1.74%	80	0.51%	0.15
A2	300	2	32.2	10Φ14	2.18%	80	0.51%	0.15
A3	300	1.5	29.4	10Φ14	2.18%	60	0.67%	0.10
A4	300	2.5	30.1	10Φ14	2.18%	60	0.67%	0.10
A5	300	2	27.3	12Φ14	2.61%	60	0.67%	0.15
A6	300	2	32.2	12Φ14	2.61%	40	1.01%	0.10

2.2. Testing Setup and Loading Sequence

The testing setup for each of the six specimens is shown in Fig.2. The specimen bottom was bolted to strong reinforced concrete foundation, at the top of the specimen was held by one vertical actuator to provide a constant axial load. Also, the specimen was loaded by two horizontal actuators which were mounted to the reaction frame.

The lateral loading history presented in Fig. 3 was applied to all specimens. The loading cycles were divided into two phases: load control and displacement control. Load control phase was used to define the piers' yield displacement Δ_y; Besides, a displacement control loading sequence was used. The displacement controlled loading history includes three complete cycles for u_Δ=1, 2, 3, ……, until the shear capacity of the piers declined to 85% of the peak loads. Here, u_Δ is the ratio of the applied lateral displacement at the top of the piers over the yield displacement Δ_y.

As shown in Figure 3(a), the first three cycles of the lateral load was applied to 70% of the theoretical yield load F_i, which was calculated based on fiber model and measured material properties. The yield displacement Δ_y was determined by extrapolating straight line from the origin through the measured point corresponding to $0.7F_i$ to the theoretical yield load F_i. The average of the values in both positive and negative loading directions was used as the yield displacement Δ_y.

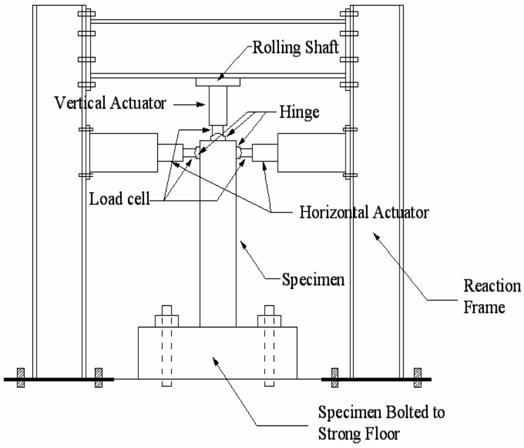

Figure 2 Testing setup

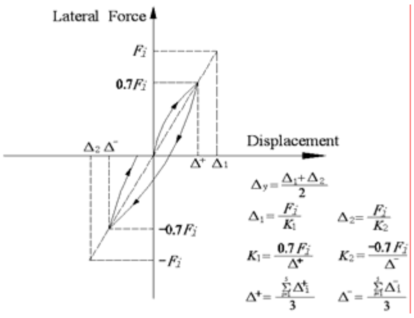

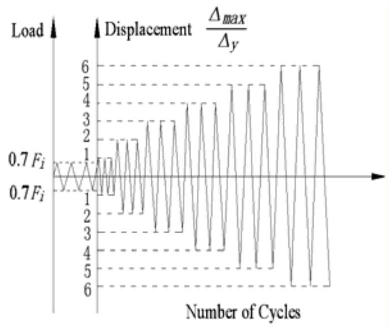

(a) Experimental definition of yield displacement (b) Loading sequence

Figure 3 Loading sequence for pier specimens

2.3. Experimental Results

The progression of damage was similar for all specimens. Flexural cracks perpendicular to the pier axis developed first in regions close to the bottom of the specimens. At later stages of loading, typically at displacement ductility levels of 2-3, the flexural cracks became inclined and extended into the neutral axis of the specimens due to the influence of shear, at the same time, initial spalling of the concrete cover was observed. Once the cover concrete had completely spalled and the spiral and longitudinal reinforcement were exposed, longitudinal bar buckling initiated within next displacement cycle. The ultimate performance of the piers were dominated by shear capacity due to concrete crushing at the bottom of the specimens, the buckling in longitudinal bars and rupturing of spiral bars. Figure 4 shows the final damage states of the specimens at the end of the tests.

Table 3 The damage parameters of the pier specimens

Specimen	Longitudinal reinforcement		Spiral reinforcement		Concrete	Exposing of
	Yielding	Buckling	Yielding	Fracture	cover spalling	reinforcement
A1	4.07mm/0.8	33.0mm/2/6.5	16.7mm/3.3		11.1mm/3/2.2	27.5mm/1/5.4
A2	3.05mm/0.7	32.8mm/1/7.3	12.8mm/2.8	36.0mm/1/8.0	12.8mm/3/2.8	24.5mm/1/5.4
A3	2.37mm/0.7	22.1mm/3/6.1	9.4mm/2.6		9.4mm/3/2.6	16.3mm/3/4.5
A4	5.62mm/0.8	50.6mm/1/7.5	16.6mm/2.5		16.6mm/1/2.5	33.0mm/3/4.9
A5	5.30mm/0.9	36.5mm/1/6.0	15.8mm/2.6	41.6mm/3/6.8	10.7mm/3/1.8	26.4mm/3/4.3
A6	4.00mm/0.6	44.4mm/3/7.0	16.8mm/2.7	49.5mm/2/7.8	11.4mm/3/1.8	38.9mm/3/6.2

Note ： a mm/b/c, a is the displacement at top of the specimen, b is cycle, c is displacement ductility factor.

New performance-based seismic design approaches aim to provided more direct consideration of a broader range of performance objectives to meet the needs of individual owners or society. It is useful to study key damage states of the piers as each damage state may be associated with one or more engineering limit states. The first occurrence of each key damage state, such as longitudinal reinforcement yielding, initial spalling of the concrete cover, spiral reinforcement yielding, exposing of spiral and longitudinal reinforcement, longitudinal reinforcement buckling, spiral fracture, is identified in Table 3.

All the lateral force-displacement responses for the specimens are shown in Fig. 10. In these figures, *Δ* indicates lateral displacement at the top of the pier and *F* is the lateral force acting on the specimen.

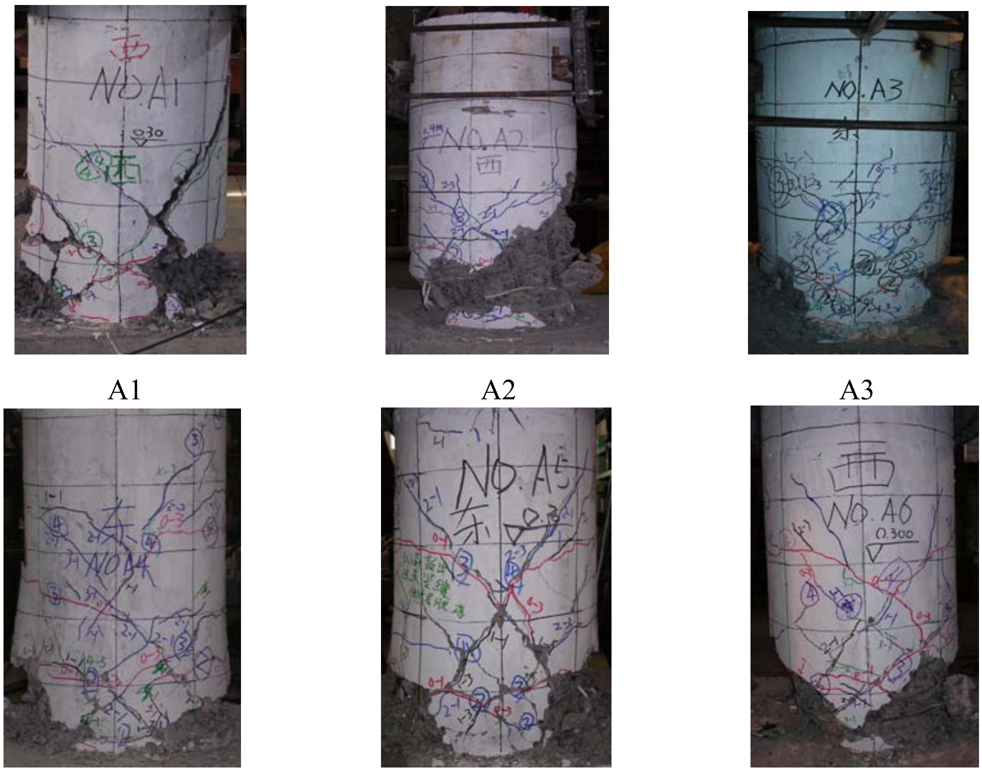

A1 A2 A3

A4 A5 A6

Figure 4 Failure patterns of the pier specimens at end of the tests

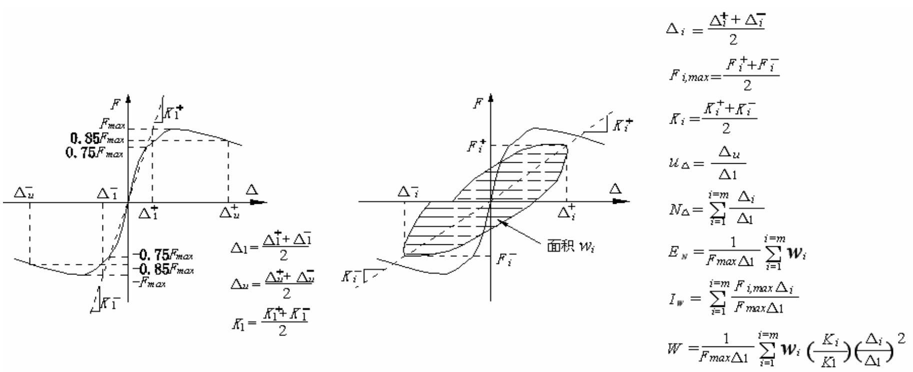

Figure 5 Define of the ductility and dissipated energy parameters of the bridge piers

In this study the ductility parameters suggested by Sheikh and Khoury (1993), Légeron and Paultre (2000) are used to evaluate the seismic performance of the specimens. Fig. 5 describes various ductility parameters that include displacement ductility factors μ_Δ, cumulative displacement ductility ratios N_Δ, normalized dissipated energy E_N, work index I_W, and work damage indicator W. The ductility factors μ_Δ and cumulative ductility ratios N_Δ represent the deformability of the member, the normalized dissipated energy E_N and work index I_W are used to assess energy dissipation capabilities, whereas the work damage indicators W estimate toughness. Table 4 lists the ductility parameters for the specimens. The results presented in Table 4 indicate that the ductility factors of the tested specimens are in the range from 5.14 to 7.48, and Specimen A6 with most transverse reinforcement has the largest ductility parameters.

Table 4 Comparison of the member ductility parameters

Specimen	$\triangle_1$(mm)	$\triangle_u$(mm)	$\mu_\triangle$	$N_\triangle$	E_N	I_W	W
A1	5.1	34.4	6.75	48.6	95.0	43.7	240.3
A2	4.5	31.2	6.93	73.3	125.0	67.3	425.6
A3	3.6	18.5	5.14	53.1	98.0	84.2	411.8
A4	6.7	48.9	7.30	86.7	158.1	79.1	579.7
A5	6.1	37.6	6.16	69.3	110.7	63.0	384.7
A6	6.3	47.1	7.48	100.2	147.3	92.7	779.6

3. NUMERICAL STUDY

To evaluate the ability of commercially available finite element analysis software ANSYS (2004) to model the hysteretic behaviour of RC bridge piers. The software ANSYS was used in the finite element analysis of the pier specimens. More specifically, the program set out to compare the load versus displacement response obtained from the computational model to those obtained from experimental results. Firstly, a series of finite element models for specimen A3 was constructed using the ANSYS software (2004) to evaluate the influence of material models and their associated parameters on the hysteretic response. Then, a modified analysis model is presented and the model accuracy has been verified by comparing the calculated hysteretic curves with experimental results.

Solid 65 elements which have crushing (compressive) and cracking (tensile) capabilities were used to model the concrete. All reinforcement were modelled using Link 8 truss elements. Solid 45 elements were used for the steel plates at the support and under the load. The effect of bond-slip at the interface between concrete elements and truss elements have been simulated using Combin39 elements.

In order to take the confinement effect into account, the Mander model (Mander et al. 1988) for confined stress-strain relationship with an assumption of perfectly plastic after ultimate compression strength was used to define the constitutive relation of concrete. Also, the concrete was modelled by a multilinear kinematic hardening relationship, using the von Mises yield criterion. The failure criterion for concrete due to multiaxial state of stress used in the study was the Willam and Warnke five parameter model, the failure surface could be defined by a minimum of two constants, f_t and f_c. Where, f_t and f_c is the concrete ultimate uniaxial tensile and the ultimate uniaxial compressive strength, respectively.

3.1. Influence of Shear Retention Coefficient

After cracking, the tension stress of the concrete element is set to zero in the direction normal to the crack plane. The shear transfer coefficient β_t for open cracks and β_c for closed cracks determines the amount of shear transferred across the cracks. The value of the shear transfer coefficient ranges from 0.0 to 1.0, with 0.0 representing no shear transfer at a crack section and 1.0 representing full shear transfer. In this study, the shear transfer coefficient (β_t) for open cracks was assumed to range from 0.2 to 0.5 while for closed cracks the shear transfer coefficient (β_c) was assumed to range from 0.5 to 0.95. As shown in Fig.6, the simulated hysteretic curves using different shear transfer coefficients are almost the same, it could be concluded that the shear transfer coefficient don't have obvious influence on the hysteretic response in this study. This may because the fixed crack model used in ANSYS software could not precisely reflect shear transfer capability across concrete cracks.

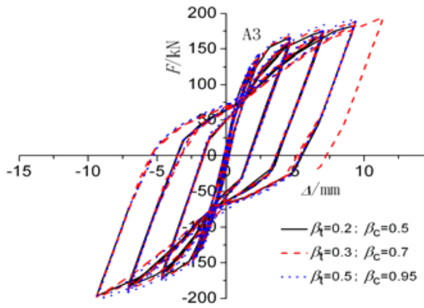

Figure 6 The influence of the shear retention coefficients to the hysteretic curves

3.2. Influence of Bauschinger Effect

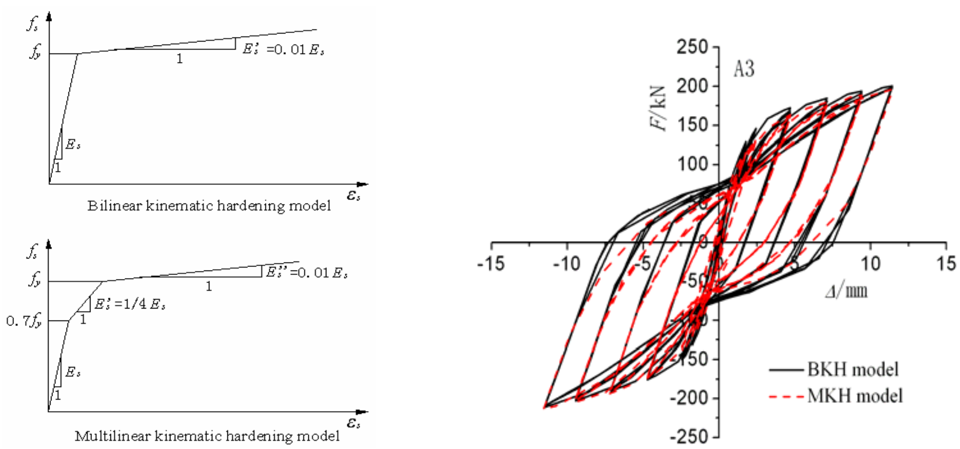

(a) Different constitutive models for reinforcing steel (b) Simulated hysteretic curves

Figure 7 The influence of different constitutive models for reinforcing steel to the hysteretic curves

Two finite element models were used to investigate the Bauschinger effect in the longitudinal reinforcement on hysteretic behaviour during cyclic loading. Bilinear kinematic hardening (BKH) model for the longitudinal reinforcement was used in model 1, whereas mltilinear kinematic hardening (MKH) model including the Bauschinger's effect was used in model 2 (Fig.7 (a)). Fig.7 (b) depicts the simulated hysteretic curves by model 1 and 2. It could be concluded that the Bauschinger effect in the longitudinal steel have a significant influence on the pinching in the hysteretic response.

3.3. Influence of Bond-Slip Effect

Two finite element models were used to investigate the effect of bond-slip on hysteretic behaviour during cyclic loading. Model 4 incorporated bond-slip modelling between the concrete and the longitudinal reinforcement whereas model 3 assumed perfect bond between them. As illustrates in Fig.8 (a), the bond-slip model for the interface element has a simplified linear relationship to the slip strength σ_c with a constant stress after the critical slip displacement Δ_c. Experimental results of the bond-slip relationship between the concrete and the longitudinal reinforcement were not available at the time of this modelling. Therefore, representative values for σ_c and Δ_c are selected as 10MPa and 0.1 mm.

Fig.8(b) depicts the simulated hysteretic curves by model 3 and 4. It is recognized that a certain degree of bond-slip may have contributed to the pinching in the hysteretic response. Also, model 4 predicts a low lateral load at large lateral displacement as a result of bond-slip effect.

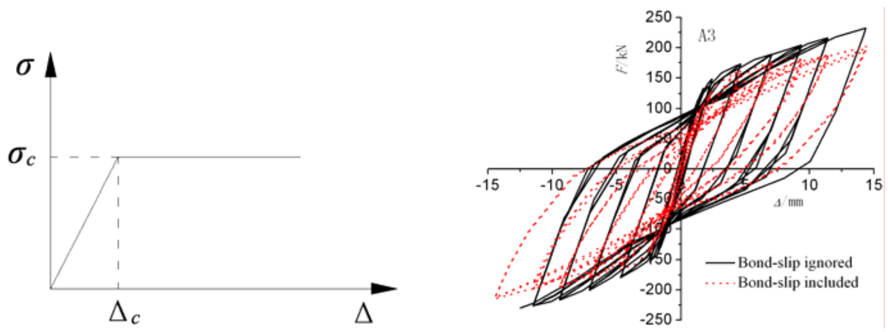

(a) The bond-slip relationship (b) Simulated hysteretic curves

Figure 8 The influence of bond-slip relationship between reinforcing steel and concrete to the hysteretic curves

3.4. Influence of Failure Surface of Concrete

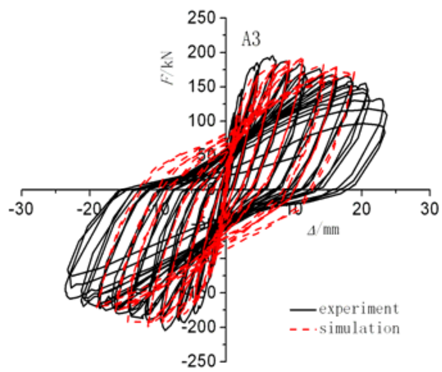

Figure 9 The influence of enlarged failure surface for concrete to the hysteretic curves

It has been reported in the literature that if both cracking and crushing capabilities are activated in ANSYS software, fictitious crushing of the concrete may be caused due to the coupling of excessive cracking strains to the orthogonal uncracked directions through Poisson's effect. This may be one of the reasons that cause divergence of the solution at later stages (Zhou et al. 2004). So in most previous literatures, the crushing capability of the concrete was turned off and the crushing failure of the concrete is ignored (Si et al. 2007).

In order to simulate the "crushing" failure of the concrete in the conducted experiments, an enlarged failure surface was used in this research, i.e. 1.2-2f_c were used to define the failure surface, but we still use normal stress-strain curves to define the constitutive relation of the concrete. Fig.9 illustrates the simulated hysteretic response by enlarged failure surface for concrete, it can be concluded that the model using enlarged failure surface of concrete predicts the pier's load-displacement relationship well.

3.5. Modified Finite Element Model

A modified finite element model is presented based on above analysis. In this model, multilinear kinematic hardening model is implemented to including the Bauschinger effect in longitudinal reinforcement, the bond-slip relationship between steel and concrete is accounted by using combin39 element, an enlarged failure surface for concrete is used to account for the confine effect by the spirals, also, it can prevent the "fictitious crushing" of the concrete. The simulated hysteretic curves are compared with experimental results, as illustrates in Fig.10, the calculated hysteretic curves are corresponding well with experimental ones.

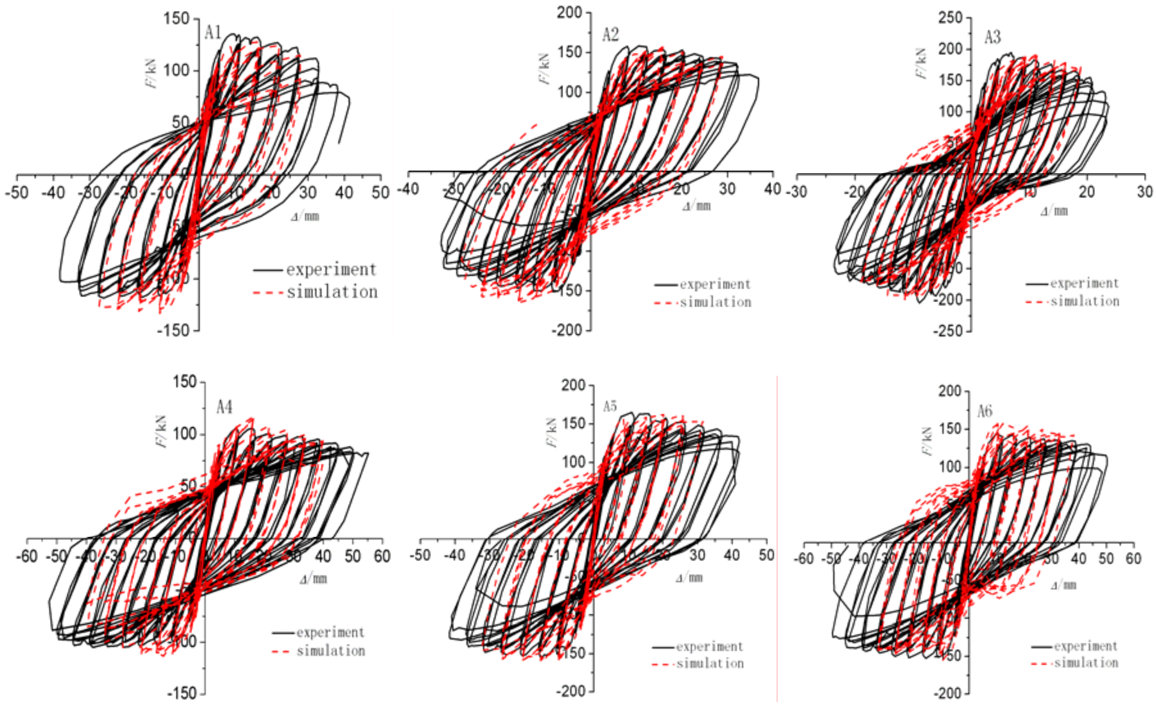

Fig.10 Comparisons of the experimental and simulated hysteretic curves

4. CONCLUSIONS

Based on the studies presented in this paper, the following conclusions can be made.

1. The progression of damage was similar for all the specimens: concrete flexural cracking, longitudinal reinforcement yielding, concrete shear cracking, concrete cover spalling, spiral reinforcement yielding, reinforcement exposing, longitudinal reinforcement buckling, and (in some cases) spiral reinforcement fracture. The ultimate performance for the piers were dominated by shear capacity due to concrete crushing at the bottom of the specimens, the buckling in longitudinal bars and rupturing of spiral bars.

2. The proposed finite element model using ANSYS software predicts the pier's hysteretic response well.

REFERENCES

ANSYS (2004), ANSYS User's Manual, ANSYS, Inc., Canonsburg, Pennsylvania, USA

Légeron F and Paultre P (2000), "Behavior of High-Strength Concrete Columns under Cyclic Flexure and Constant Axial Load," *ACI Structural Journal*, **97(4)**: 591-601

Mander J B, Priestley M J N and Park R (1988), "Theoretical Stress-Strain Model for Confined Concrete," *Journal of Structural Engineering*, ASCE, **114(8)**: 1804-1826

Sheikh S A and Khoury S S (1993), "Confined Concrete Columns with Stubs," *ACI Structural Journal*, **90(4)**: 414-431

Si Bingjun, Sun Zhiguo and Ai Qinghua (2007), "Application of Solid65 Element in the Finite Element Analysis of Concrete Structures," *Industrial Construction*, **37(1)**: 87-92. (in Chinese)

Zhou S, Rizos D C and Petrou M F (2004), "Effects of Superstructure Flexibility on Strength of Reinforced Concrete Bridge Decks," Computers & Structures, **82(1)**: 13-23